

## Stress concentration targeted reinforcement using multi-material based 3D printing

Himanshu Singh <sup>a,1</sup>, Aelton B Santos <sup>b,1</sup>, Diptava Das <sup>a</sup>, Rushikesh S. Ambekar <sup>a</sup>, Prateek Saxena <sup>c</sup>, Cristiano F. Woellner <sup>b,\*</sup>, Nirmal Kumar Katiyar <sup>a,d,\*\*</sup>, Chandra Sekhar Tiwary <sup>a,\*\*\*</sup>

<sup>a</sup> Department of Metallurgical and Materials Engineering, Indian Institute of Technology, Kharagpur, West Bengal 721302, India

<sup>b</sup> Department of Physics, Federal University of Paraná UFPR Curitiba-PR, 81531-980, Brazil

<sup>c</sup> School of Mechanical and Materials Engineering, Indian Institute of Technology, Mandi, Himachal Pradesh 175005, India

<sup>d</sup> Amity Institute of Applied Sciences, Amity University Noida, Sector 125, Uttar Pradesh 201303, India

### ARTICLE INFO

**Keywords:**

Flexible material  
Multi-material  
Finite element analysis  
3D printing  
Schwarzite

### ABSTRACT

Topological engineering (3D printing into complex geometry) has emerged as a pragmatic approach to develop high specific strength (high strength and low density) lightweight structures. These complex lightweight structures fail at high-stress concentration regions, which can be replaced with soft/tough material using 3D printing. It can improve mechanical properties such as strength, toughness and energy absorption etc. Here, we have developed stress concentration targeted multi-material schwarzite structures by 3D printing technique. The soft (Thermoplastic Polyurethane) material is reinforced at high-stress concentration regions of hard (Polylactic acid) schwarzite structures to enhance the specific yield strength and resilience. The mechanical properties and responses of these structures were then assessed via uniaxial compression tests. The multi-materials 3D printed composite structure shows improved mechanical properties compared to single materials architecture. The specific resilience of composites demonstrates remarkable enhancements, with percentage increases of 204.70 %, 596.50 %, and 1530.99 % observed when compared to hard primitives, and similarly impressive improvements of 182.45 %, 311.64 %, and 477.75 % observed in comparison to hard gyroids. The obtained experimental findings were comprehensively examined and validated with molecular dynamics (MD) simulations. The promising characteristics of these lightweight multi-material-based Schwarzites structures can be utilized in various fields such as energy harvesting devices, protective, safety gears, and aerospace components.

### 1. Introduction

The composite approach (*i.e.* reinforcing hard/soft materials into a soft/hard matrix) leads to an improvement in mechanical properties that lie in between the individual properties of its component [1,2]. From a materials design perspective, the strength and ductility/plasticity of the composite are governed by the load/stress or strain transfer from the matrix to the reinforcement and vice versa [3,4]. Engineering the topology of the composite and reinforcing the hard/soft materials at site-specific can outshine the conventional materials design paradigm [5–7]. The recent advancement in additive manufacturing/3D printing enables us to intricately engineer designs through a meticulous

layer-by-layer deposition process of different hard and soft materials, hybrid materials bioprinting, etc. [1,8–12]. It can also fabricate multi-material complex architecture with site-specific deposition of different materials (with different mechanical/chemical properties as compared to matrix), which can result in enhanced mechanical properties compared to the individual components (matrix/reinforcement) [13–15]. However, the orientation of the building process in 3D printing significantly influences the bonding at interfaces and exhibits anisotropic characteristics when subjected to compression testing. This effect is particularly noticeable in composite materials [16]. Conversely, a variety of experiments were conducted to assess and improve the interface between two layers using lap joint strength testing [17]. These

\* Corresponding author.

\*\* Corresponding authors at: Department of Metallurgical and Materials Engineering, Indian Institute of Technology, Kharagpur, West Bengal 721302, India.

E-mail addresses: [woellner@ufpr.br](mailto:woellner@ufpr.br) (C.F. Woellner), [nkumar22@amity.edu](mailto:nkumar22@amity.edu) (N.K. Katiyar), [chandra.tiwary@metal.iitkgp.ac.in](mailto:chandra.tiwary@metal.iitkgp.ac.in) (C.S. Tiwary).

<sup>1</sup> These authors contributed equally to this work.

tests encompassed variations in layer thickness, complex geometries, different adhesive materials, varying loading rates, and the incorporation of carbon nanotubes into polymer composite printing [17,18].

The team consisting of theoreticians and experimentalists have utilized 3D printing to fabricate several complex architectures inspired by atomic scale framework [19–23], nature/bio-mimetic [24] mathematical model [25,26] etc. Most of these structures exhibit unique stress/strain distribution, which results in enhanced mechanical properties such as specific strength, high plasticity and toughness/energy absorption [22,23,27,28]. Among all the 3D printed architecture, the three-dimensional carbon structure with negative Gaussian curvature (Schwarzites) has attracted a lot of attention due to its unique physical and topological properties. The *in-situ* deformation studies reveal that the load-bearing capacity of both primitive and gyroid schwarzite

structures is dependent on the presence of stress concentration regions, where the von Mises stress exceeds the sample's yield strength. Previous research [18] has shown that premature failure/crack initiation in these structures occurs at sharp corners during compression testing, resulting in a degradation of their mechanical properties. To enhance their mechanical properties, one potential approach is to employ multi-material 3D printing to replace the localized stress-concentrated regions with a material characterized by high toughness. The enhanced properties are utilized in several applications such as impact resistance structures [29], energy harvesting, water/environmental cleaning [30], catalysis [31] etc. In the realm of literature, substantial progress has been witnessed in software development, including advancements in G-code files [32], the introduction of portable 3D bioprinters [33], the integration of machine learning in the context of 3D printing and bioprinting [34], as well as the

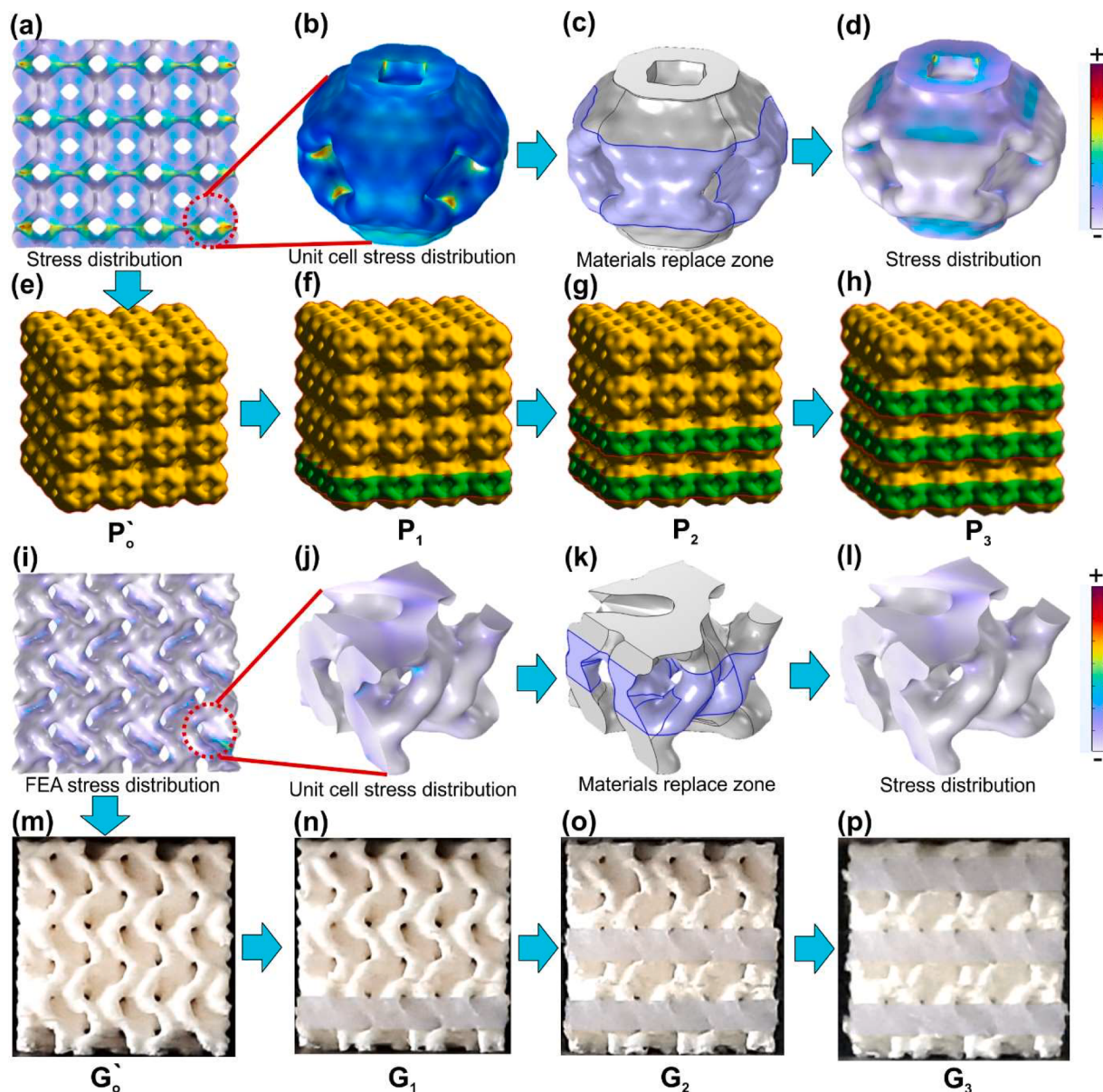


**Fig. 1.** Process schematics and 3D printed Primitive and Gyroid Schwarzites (a) Primitive structure von Mises stress concentration zone by FEA simulation. (b) Von-Mises stress concentration in the single unit cell of primitive. (c) schematics high-stress zone materials replaced section marked in the single unit cell. (d) Von-Mises stress concentration in the single unit cell of primitive after replacing TPU materials. (e-h) Primitive structure materials were replaced in a layered manner and renamed each kind structure  $P_0$ ,  $P_1$ ,  $P_2$  and  $P_3$ . (i) Gyroid structure von Mises stress concentration zone by FEA simulation. (j) Von-Mises stress concentration in the single unit cell of the gyroid. (k) Schematics high-stress zone materials replaced the section marked in the single unit cell. (l) Von-Mises stress concentration in the single unit cell of gyroid, after replacing TPU materials. (m-p) optical photograph of gyroid structure materials replaced in a layered manner and renamed each kind structure  $G_0$ ,  $G_1$ ,  $G_2$  and  $G_3$ .

exploration of diverse bioprinting techniques and the printing of composite hybrid materials [35].

In this study, a pragmatic approach involving a combination of soft (e.g. Thermoplastic polyurethane (TPU)) and hard (e.g. Polylactic acid (PLA)), have been 3D printed, which employed the material extrusion (MEX) based additive manufacturing technique in accordance with the ISO/ASTM52900-21 standard [36,37]. The compressive mechanical tests were performed on the 3D printed structures, and the results were corroborated with the help of molecular dynamics studies. The selective incorporation of soft materials allows us to balance between elasticity/ultimate strength with resilience/energy absorption of the Schwarzeite structures. The FEA analysis has been performed to identify the stress-concentrated region and then replace it with soft materials using 3D printing. The FEA analysis of the multi-materials 3D printed structure has been performed to understand the role of the soft materials deposition at site-specific regions for stress/strain localization. This study will open up new vistas to identify the high-stress regions in the complex structure and replace those critical regions with soft and tough materials using fine-controlled 3D printers. This approach is particularly advantageous in engineering applications with lightweight yet robust components, such as aerospace, automotive, and energy harvesting devices, which are essential.

## 2. Experimental details

The theoretical atomic scaled model for primitive and gyroid schwarzites is developed for this study denoted by P and G respectively (as shown in Fig. 1). The porous P structure comprises 192 carbon atoms and 5184 supercells, while the porous G structure comprises 384 carbon atoms and 3072 supercells [23]. These nanoscale structures are then scaled to the macroscale and subsequently used for 3D printing. Finite Element Analysis (FEA) simulation was used to identify high-stress concentration regions within these porous structures. The high-stress regions from the FEA study were selected and printed using TPU (Soft). The von Mises stress distribution on the front and back side of schwarzite, and highlights the high stress concentration region, as described in Fig. S2.

The 3D printing of the structures was done using a dual-nozzle fused deposition modelling-based printer (Flashforge Creator Pro), schematics are shown in Supplementary Information Fig. S1. The accuracy of the fabricated samples primarily depends on the printing process parameters. We printed the complex structures using the optimised printing process parameters, including a layer thickness of 100  $\mu\text{m}$ , a print precision of  $\pm 200 \mu\text{m}$ , a base print speed of 40 mm/sec, a travel speed of 70 mm/sec, 100 % fill density, and 3D infill patterns provided by the Flashforge Creator Pro 3D printer. After 3D printing, we measured the dimensions, which closely approximated the CAD model. To compare structural performance, the dimensions of the CAD model (FEA) and the 3D printed structure are similar. There are a limited number of hard polymers, such as Polylactic Acid (PLA), Acrylonitrile Butadiene Styrene (ABS), Polyethylene Terephthalate Glycol (PETG), Nylon, etc. having excellent rigidity. Soft polymers such as Thermoplastic Polyurethane (TPU), Thermoplastic Elastomer (TPE), and Thermoplastic Copolyester (TPC) polymers have high elasticity, outstanding abrasion resistance, and flexibility, available for 3D printing. The selection of hard and soft polymers is based on mechanical properties, cost, eco-friendliness and ease of fabrication. Hence, we have taken PLA and TPU as filament materials for multi-material-based 3D printing.

The printing process involved feeding commercial-grade solid PLA and TPU filaments into the printer, procured from WOL 3D, India. The left nozzle is assigned to extrude TPU whereas, the right nozzle is assigned to extrude PLA (Hard). The material fed in the 3D printer in the form of a filament having a 1.75 mm consistent diameter. The mass densities of TPU and PLA are 1.21 g/cm<sup>3</sup> and 1.27 g/cm<sup>3</sup> respectively. TPU filament was heated in the extruder nozzle at 230°C, while PLA filament was heated at 210°C. These materials were extruded through a

nozzle onto a heated print bed at 50°C. The fabricated structures had a single-layer thickness of 110  $\mu\text{m}$  along the z-direction (vertical direction) and a 100 % infill density. In the context of multi-material extrusion-based printing, when the printing process begins, nozzles operate at different temperatures. When the nozzle with PLA filament is extruding, and the other nozzle with TPU remains idle, molten TPU material can ooze from the nozzle, and vice versa. This oozing phenomenon can come into contact with the printed part, potentially compromising the printing process. To address this issue, we have introduced protective walls around the printed object using Flashprint software. These walls effectively contain the oozing material, ensuring a smoother multi-material printing process.

The compression testing of the 3D printed structures was conducted on a UTM TINIUS 60T machine, and the load-bearing capacity of the structures was measured along the perpendicular direction of the layer printing direction, specifically in the Z-direction, as shown in supplementary information Fig. S3. All samples were prepared in three sets, and average data has been presented of three replications, the standard deviation of results are lies within 5 %. A constant strain rate of 2 mm/min was applied during the compression testing. Finite element analysis (FEA) was performed using the structural engineering module of COMSOL Multiphysics. An optical camera is positioned in front of the sample during the compression test to observe and analyze the deformation behaviour of the printed specimens.

The molecular dynamics simulation has been performed for all the structures to deduce the underlying mechanism of deformation. The unit cell Lattice and parameters used in the calculation have been provided in the Supplementary Information Table S1. The structure used was a  $4 \times 4 \times 4$  supercell, parameters for the unit cells were extracted from the research of Terrones et al. [38]. Subsequently, these parameters were employed in VESTA [39], a 3D visualization tool for crystal structures, to generate Crystallographic Information Framework (CIF) files utilized in the lammps-interface tool [40]. By utilizing the lammps-interface, we automatically obtain the coefficients required for our systems based on the chosen force field, in this case, Universal Force Field (UFF) [41]. The Universal Force Field (UFF) is a widely used classical force field introduced in 1992 as a general-purpose force field applicable to all atoms in the periodic table, parameterized using general rules based only on the element, hybridization and connectivity. In UFF the bond stretch is described by a harmonic oscillator, with the natural bond length and bond dissociation energy being the parameters. The angle bend and the torsional terms for two bonds are both described as a cosine Fourier expansion in  $\Theta$  and  $\phi$  respectively. Two sets of atoms were created using VMD, a powerful and widely used molecular visualization software. One group represented the "soft" material, comprising unchanged carbon atoms, while the other group represented the "hard" material, where the carbon atoms had their bond, angle, dihedral, and improper coefficient energies modified by a 20 times multiplier. This resulted in two materials with varying levels of hardness, which were then ready to be combined. These atom groups were designed to replicate the different materials used in the experiment, leading to the creation of the structures depicted in Fig. 3. and S5.

Subsequently, for the molecular dynamics simulations, we utilized the molecular dynamics simulator LAMMPS (Large-scale Atomic/Molecular Massively Parallel Simulator). To set up the simulations, we employed the selected force field and generated the necessary data for LAMMPS using the lammps-interface tool previously mentioned. Following the generation of the structures, LAMMPS input files were prepared to define the simulation process. The systems underwent an initial thermalization step before being subjected to strain, where they were deformed at a constant rate. During this process, the von Mises stress was calculated using the formula outlined in Eq. 1.

$$\sigma_{vm} = \sqrt{[0.5[(\sigma_{xx} - \sigma_{yy})^2 + (\sigma_{yy} - \sigma_{zz})^2 + (\sigma_{zz} - \sigma_{xx})^2] + 3(\sigma_{2xy} + \sigma_{2yz} + \sigma_{2zx})]} \quad (1)$$

$\sigma_{vm}$ : Components of the stress tensor.

### 3. Results and discussions

Initially, the von Mises stress concentration or high-stress zones in primitive and gyroid schwarzite structures have been analyzed, as shown in Fig. 1a. A stationary study was adopted and Fine mesh size for proper meshing, (more detail in supplementary information Fig. S2, Table S2 and Table S3. In this FEA simulation, a uniform displacement boundary condition was applied at the bottom portion of the structure, while a fixed boundary condition was applied at the top portion and the

PARDISO solver and pivoting perturbation  $1e^{-9}$ , were selected for analysis. In case of linear elastic material, Hooke's law relates the stress tensor to the elastic strain tensor. The governing mathematical equations are described in the supporting information Eq (S1-4).

This setup allowed for the simulation of the structural response under compression. Fig. 1b, j illustrates the results of the FEA simulation of the schwarzite structures, with the von Mises stress distribution represented by a colour code. In this representation, red indicates high-stress concentration regions/ yield strength of the sample, while light blue represents regions with lower stress concentration. The analysis outcomes revealed that schwarzite structures displayed a notable

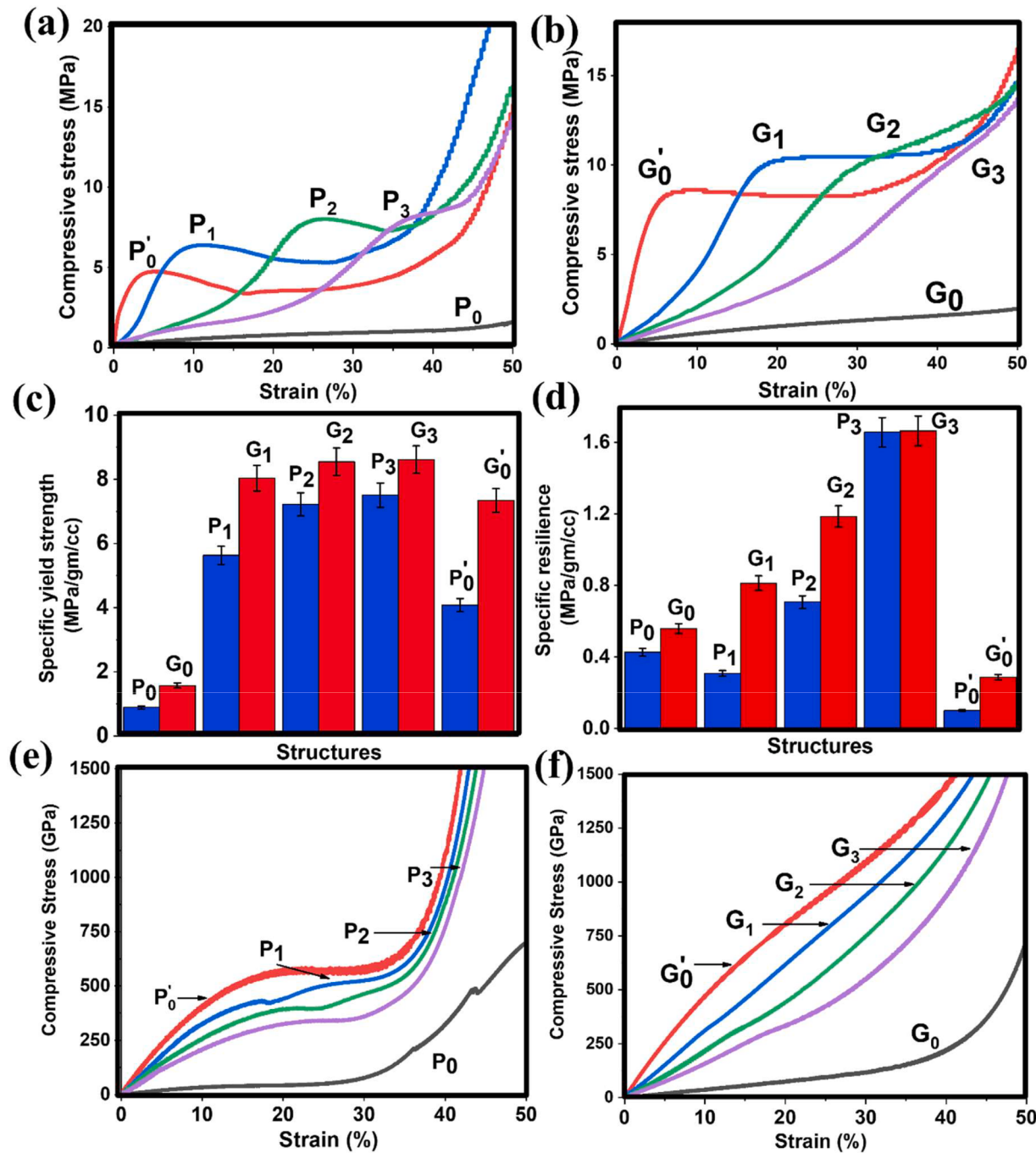


**Fig. 2.** Compressive stress-strain curves for schwarzites (a) Primitive schwarzites multi-material structures stress-strain curve. (b) Gyroid schwarzites multi-material structure stress-strain curve. (c) Comparison of specific yield strength of all schwarzite structures, (d) comparison of specific resilience of all schwarzites. (e) Stress-strain curve theoretically calculated by molecular dynamics for primitive schwarzites. (f) Stress-strain curve theoretically calculated by molecular dynamics for gyroid schwarzites.

localization of high-stress concentration at the bulge section of the unit cell, as visually depicted in Fig. 1b. Similarly, within the gyroid structure, intensified stress concentration emerged at the sharp corners of the unit cell, as illustrated in Fig. 1j. The gyroid schwarzite shows more uniform stress distribution compared to the primitive schwarzite, as shown in Fig. 1b and j. To counteract this concern, the high-stress concentration zone was substituted with the TPU, in both the structures. The incorporation of TPU in specific areas helps in alleviating localized stress concentration. Consequently, it led to an enhancement in structural integrity and averted premature structural failure. This FEA analysis provided valuable insights into the stress distribution and concentration within the primitive and gyroid structures.

Further, all structures were printed as mentioned in Fig. 1, schwarzites ( $P_0$ ,  $P_1$ ,  $P_2$ ,  $P_3$ , and  $P'_0$ ) and gyroids ( $G_0$ ,  $G_1$ ,  $G_2$ ,  $G_3$  and  $G'_0$ ), details shown in supplementary information Fig. S3. The load-bearing capacity of 3D printed structures is measured along the perpendicular direction of the layer printing (Z-direction) at a constant compression rate of 2 mm/min. The resulting compressive stress-strain curves were obtained for different volume fractions of TPU in the composite, specifically targeting the identified high-stress concentration locations determined through FEA analysis.

Fig. 2a,b shows the compressive stress-strain curves comprising primitives, gyroids, and their various multi-material composites. Within these graphs, both structures were fabricated using pristine TPU and pristine PLA. Specifically, the pure variants of TPU were denoted as  $P_0$  and  $G_0$ , while the pure counterparts of PLA were labelled as  $P'_0$  and  $G'_0$ . Interestingly, the structural integrity of the pure material versions exhibited notably lower specific yield strength and energy absorption characteristics than composites. Furthermore, the unaltered robust PLA faced failure owing to zones of elevated stress concentration, particularly evident at sharp corners. This phenomenon led to an untimely breakdown of structural integrity. The mechanical responses such as specific yield strength (yield strength/density), specific resilience (area under the curve up to elastic limit/density) and specific energy absorption (area under the curve up to 50 % strain/density) are estimated for the analysis [42]. In the composite materials design, a significant observation emerges: when the soft phase ( $P_0$  or  $G_0$ ) volume fraction within the hard phase ( $P'_0$  or  $G'_0$ ) is increased, there is a corresponding augmentation in both yield strength and percentage strain, as depicted in Fig. 2a,b. The mechanical properties such as specific yield strength, and specific energy absorption results for PLA-based porous primitive ( $P'_0$ ) and gyroid ( $G'_0$ ) schwarzites are described in Fig. 2a,b. These mechanical responses of primitive and gyroid schwarzites align with the findings of Sajadi et al [23].

The 14 % volume fraction of TPU incorporated in the matrix of PLA in the form of a sandwich named  $P_1$ , exhibited a remarkable increase of 531.46 % in specific yield strength and 699.77 % in specific energy absorption compared to the flexible schwarzite ( $P_0$ ). It also displayed a 38.16 % increase in specific yield strength and a 59.08 % increase in specific energy absorption compared to the hard schwarzite ( $P'_0$ ). Further, increasing the materials A volume fraction to 28 % in the composite, the schwarzite composite ( $P_2$ ) demonstrated a 709.73 % increase in specific yield strength and a 546.78 % increase in specific energy absorption compared to the flexible schwarzite ( $P_0$ ), the comparison has shown in Fig. 2c.

It also showed a 77.16 % increase in specific yield strength and a 28.65 % increase in specific energy absorption compared to the hard primitive schwarzite. Additionally, by adding a 41 % volume fraction of TPU in the composite,  $P_3$  exhibited an 84.21 % increase in specific yield strength compared to  $P'_0$ , as shown in Fig. 2c. The specific resilience of the composite materials ( $P_1$ ,  $P_2$  and  $P_3$ ) shows remarkable improvements of 204.64 %, 596.50 %, and 1530.99 %, respectively, compared to  $P'_0$ , as illustrated in Fig. 2d, and Fig. S4e,f. In comparison of primitive and gyroid, the gyroid always shows superior resilience as well as yield strength as shown in Fig. 2c-d. This was also confirmed in the FEA simulation, the gyroid topology distributes the stress more uniformly

than primitive topology. The Gyroid structure's results have been discussed in detail in supplementary information.

The specific energy absorption of all samples has been summarized in Fig. S4a-d comparing theoretical with the experimental results. The addition of TPU in composite results in a significant increase in their energy absorbing capacity, as depicted in Fig. S4a-d. These findings indicate that the incorporation of TPU enhances the ability of the composites to absorb and store elastic energy, making them more resilient and suitable for applications where energy absorption and recovery are crucial. However, it showed a decrease in specific energy absorption capacity at higher volume fractions of TPU, as shown in Fig. S4a, b. Furthermore, opting for a non-reactive force field to describe the interactions implies that, essentially, the molecular dynamics systems are perpetually operating within the elastic limit. As a result, the enhanced recovery of the composite material is not accurately depicted. There was no large difference observed in the variants of samples. Despite the differences, the stress-strain profile is similar to the experimental.

### 3.1. Deformation mechanisms

When examining the compression deformation mechanisms of porous structures made of pristine TPU, PLA, and composite structures combining both materials, several important factors affect the mechanical properties. In the context of molecular dynamics (MD) simulation, the deformations of the structures are meticulously captured at each procedural step. Similarly, a parallel depiction of progressive structural deformation is showcased through optical photographs in the experimental setup. This visual comparison is outlined in Fig. 3 for primitive schwarzites, while for the gyroid schwarzites, a corresponding representation can be found in Fig. S5 within the supplementary information. The deformation behaviour during compression test of primitive and gyroid schwarzite structures can be seen in Supplementary information SV1, SV2, SV3and SV4 respectively. Initially, both the porous TPU and PLA undergo elastic deformation when subjected to compressive loads. The  $P_0$  and  $G_0$  exhibit 98 % shape recovery after unloading but this phenomenon is not observed in hard materials ( $P'_0$  and  $G'_0$ ) as shown in supplementary information Fig. S4g,h. However, as the compressive load increases, the porous PLA ( $P_0$ ) reaches its elastic limit, leading to plastic deformation.

In the case of  $P'_0$  the initial cracks start from the right bottom domain then the bulge domain collapses and in  $G'_0$  the initial cracks start from the right bottom domain, as displacement is applied from the bottom surface. The presence of a high-stress concentration zone in this hard PLA, is responsible for crack propagation, which leads to premature fracture of this structure, as shown in Fig. 4a. This phenomenon is confirmed by the FEA analysis. In composite structures, when flexible TPU is strategically positioned to replace the regions of higher stress concentration within the rigid PLA, hence remarkable deformation mechanism can be observed. In the distribution of mechanical stresses between TPU and PLA, the TPU contributes to load sharing at the interface of the composites, as shown in Fig. 4b. This phenomenon plays a crucial role when TPU replaces PLA in a composite at high-stress concentration regions. Stress is caused by the application of external load and initially affects the PLA matrix before gradually moving to the interface and then TPU. This soft material can deform more easily under stress and usually has a larger strain accommodation capacity, as shown in Fig. 4c. They undergo controlled deformation when placed in high-stress concentration regions, which allows them to absorb a significant proportion of the applied load. This stress re-distribution promotes a uniform load distribution and prevents localized stress concentration. Prudent material selection and design are essential for maximizing load sharing and enhancing overall composite performance because the soft material's capacity for stress relaxation/strain accommodate and energy absorption helps in the prevention of sudden failure. Therefore, specific resilience and overall mechanical performances of the composite

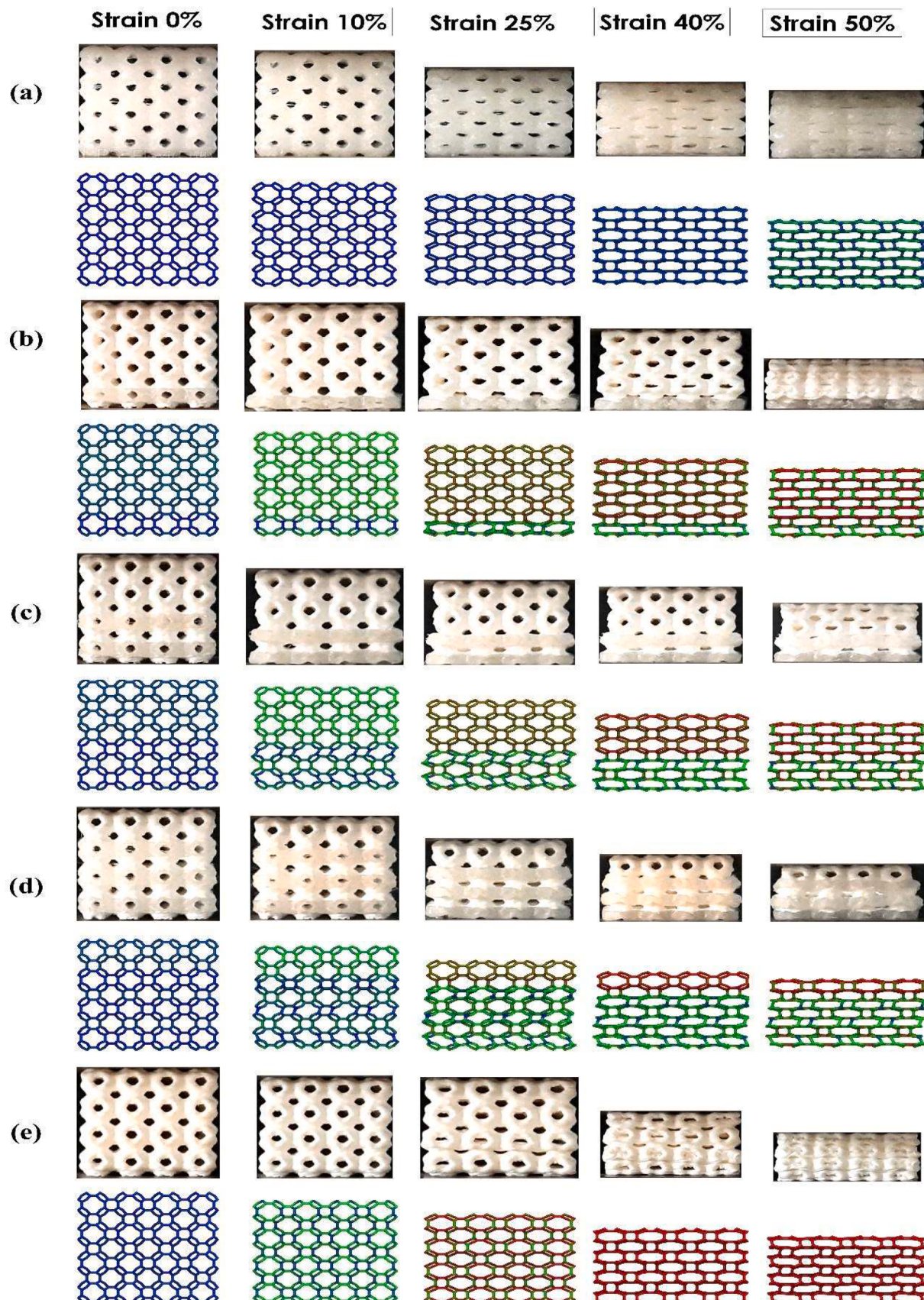


**Fig. 3.** Progressive deformation at different levels of strain(a) Deformation of pristine materials type A.(b)Deformation of composite P<sub>1</sub>.(c) Deformation of composite P<sub>2</sub>.(d) Deformation of composite P<sub>3</sub>.(e) Deformation of composite P<sub>0</sub>.

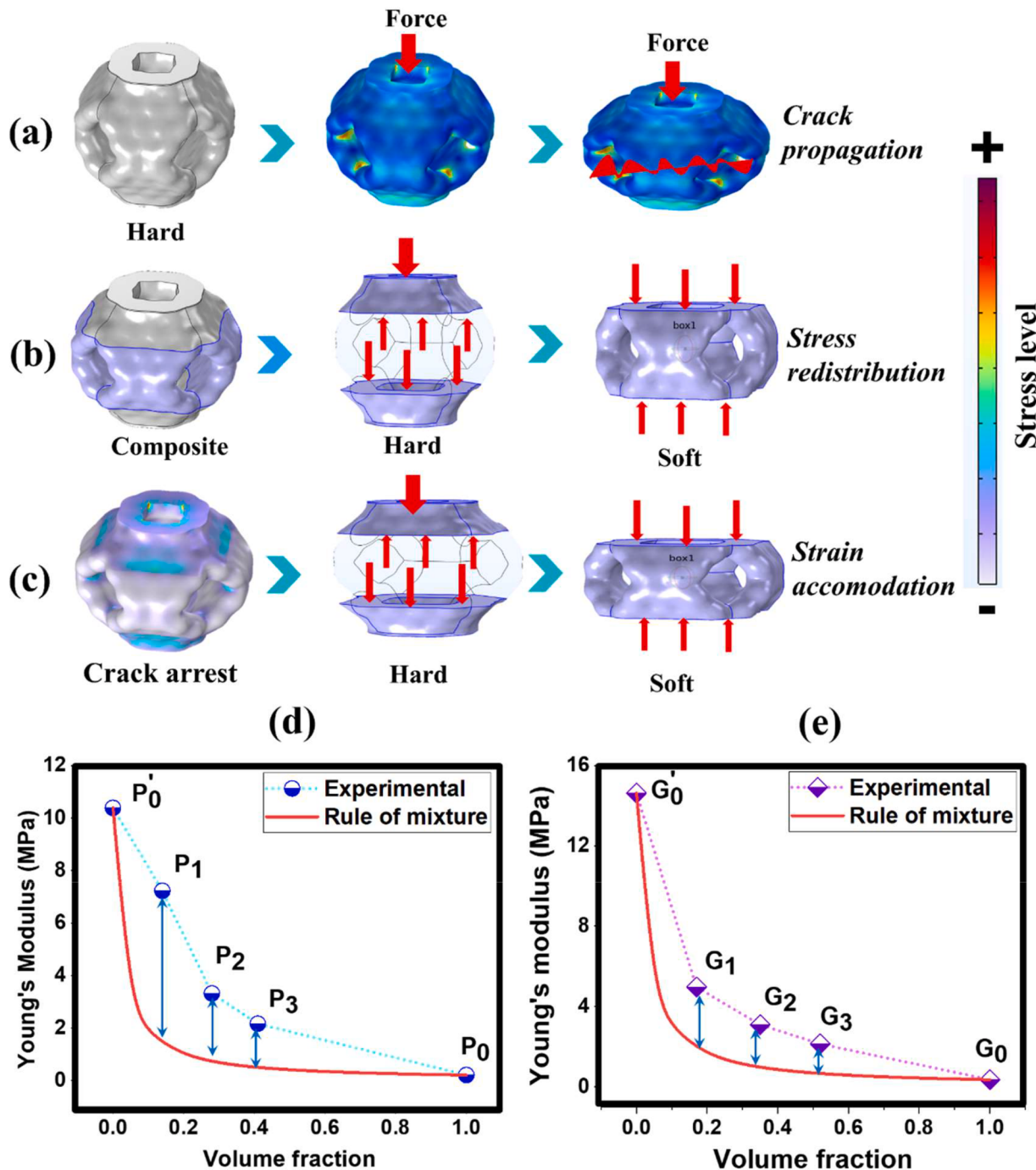


**Fig. 4.** Effect of hard and soft materials blending (a) The propagation of cracks within the high-stress concentration region in the hard PLA. (b) Redistribution of stress at the interface between the hard and soft phases. (c) Regions of stress dissipation and stress relaxation within the composite structures. (d-e) A comparison between the experimental Young's modulus and the Young's modulus predicted by the rule of mixture for both the Primitive and Gyroid families.

experience an improvement as shown in Fig. 3c-e and supplementary information in Fig. S5c-e. The interface between PLA and TPU materials primarily focuses on strain accommodation during uni-axial compression. However, mitigating the impact of shear forces between the interfacial layers poses a significant challenge. To overcome this issue, a unique method for enhancing interfacial bonding quality by employing inter-layer insets and in-layer overlap configurations, ultimately enhancing the mechanical performance of multi-material-based composites [16].

The elastic energy storage inside the soft material during loading is responsible for the shape recovery phenomena, as shown in Fig. S4g,h. In addition to preserving the integrity of the composite, recovery of

shape helps to redistribute stress and minimise the buildup of excessive stress levels. Due to this characteristic, the composite can be more resilient to cyclic loading and is a suitable choice for applications employing dynamic or fluctuating mechanical stresses [43].

Further, experimental findings are discussed based on the rule of mixture. The Young's modulus of the composites was determined by measuring the slope of the stress-strain curves, as presented in Tables S4 and S5 in the Supporting information. Additionally, Young's modulus values were computed using the rule of mixtures for transverse loading conditions, described by Eq. 1 and plot shown in Fig. 4d,e. The mechanical properties of experimental results show synergistic improvement compared to those predicted by the rule of mixtures because of the

structural gain Fig. 4d,e. This phenomenon can be attributed to stress transfer mechanisms not accounted for in the theoretical model. The quality of the interface adhesion between the hard matrix and the soft can be a crucial factor influencing the mechanical properties of the composite. In experiments, the actual adhesion strength and material compatibility at the interface significantly impacted the composite's overall stiffness, contributing to a higher Young's modulus.

$$E_c = \frac{E_A E_B}{E_A v_B + E_B v_A} \quad (2)$$

Where  $E_c$  is Young's modulus of the composites  
 $E_A$  and  $E_B$  are Young's modulus of the TPU and PLA  
 $v_B$  and  $v_A$  are Volume fractions of the TPU and PLA

#### 4. Conclusions

In summary, Finite element analysis (FEA) successfully predicted high-stress concentration areas within schwarzite and gyroid structures. During 3D printing experiments, substituting hard materials with a soft layer in regions of high-stress concentration enhanced mechanical performance without resulting in failure. The synergistic effects observed in this study highlight the importance of precise stress concentration targeting technique, improving the stress redistribution and strain accommodation/energy absorption in the soft domain, leading to enhanced Young's modulus compared to the rule of mixture result. This adjustment essentially involves a balance between flexibility and strength. The specific resilience of composites demonstrates remarkable enhancements, with percentage increases of 204.70 %, 275.28 %, and 1326.74 % observed when compared to hard primitives, and similarly impressive improvements of 182.45 %, 311.64 %, and 477.75 % observed in comparison to hard gyroids. The developed class of composites exhibits a paradigm shift from conventional design by incorporating different volume fractions of soft material into hard material. Selective reinforcement in schwarzites composite design reduces the risk of sudden failure, possess broad applications in aerospace, automotive, energy harvesting, and electronics field.

#### CRediT authorship contribution statement

**Himanshu Singh:** Investigation, Validation, Formal analysis, Project administration, Visualization, Writing – original draft, Data curation, Software. **Aelton B Santos:** Software, Validation, Visualization. **Diptava Das:** Data curation, Software. **Rushikesh S. Ambekar:** Formal analysis, Writing – review & editing. **Prateek Saxena:** Software. **Cristiano F. Woellner:** Methodology, Software, Supervision. **Nirmal Kumar Katiyar:** Supervision, Visualization, Writing – review & editing. **Chandra Sekhar Tiwary:** Conceptualization, Writing – review & editing, Funding acquisition, Supervision, Resources.

#### Declaration of Competing Interest

The authors declare that they have no known competing financial interests or personal relationships that could have appeared to influence the work reported in this paper.

#### Data availability

Data will be made available on request.

#### Acknowledgements

C.S.T acknowledges Core research grant of SERB, India, STARS projects by MHRD-India, DAE Young Scientist Research Award (DAEYSRA), and AOARD (Asian Office of Aerospace Research and Development) grant no. FA2386-21-1-4014, and Naval research board

for funding support (FA2386-23-14034).

#### Supplementary materials

Supplementary material associated with this article can be found, in the online version, at doi:10.1016/j.apmt.2023.102010.

#### References

- [1] Y. Zhang, F. Zhang, Z. Yan, Q. Ma, X. Li, Y. Huang, J.A. Rogers, Printing, folding and assembly methods for forming 3D mesostructures in advanced materials, *Nat. Rev. Mater.* 2 (2017) 17019, <https://doi.org/10.1038/natrevmats.2017.19>.
- [2] Y. Wei, Y. Li, L. Zhu, Y. Liu, X. Lei, G. Wang, Y. Wu, Z. Mi, J. Liu, H. Wang, H. Gao, Evading the strength–ductility trade-off dilemma in steel through gradient hierarchical nanotwins, *Nat. Commun.* 5 (2014) 3580, <https://doi.org/10.1038/ncomms4580>.
- [3] X. Zhao, Y. Long, S. Xu, X. Liu, L. Chen, Y.Z. Wang, Recovery of epoxy thermosets and their composites, *Mater. Today* 64 (2023) 72, <https://doi.org/10.1016/j.mattod.2022.12.005>.
- [4] J. Shen, X. Lin, J. Liu, X. Li, Revisiting stress-strain behavior and mechanical reinforcement of polymer nanocomposites from molecular dynamics simulations, *Phys. Chem. Chem. Phys.* 22 (2020) 16760, <https://doi.org/10.1039/DQCP02225J>.
- [5] A. Goulas, T. Whittaker, G. Chi-Tangye, I.M. Reaney, D. Engström, W. Whittow, B. Vaidyanathan, Multi-material additive manufacture and microwave-assisted sintering of a metal/ceramic metamaterial antenna structure, *Appl. Mater. Today* 33 (2023), 101878, <https://doi.org/10.1016/j.apmt.2023.101878>.
- [6] A. Zhakeev, M. Abdulrhman, Y. Zhang, F. Li, G. Chen, J. Marques-Hueso, Upconversion 3D printing enables single-immersion multi-material stereolithography, *Appl. Mater. Today* 32 (2023), 101854, <https://doi.org/10.1016/j.apmt.2023.101854>.
- [7] A. Dixit, M. Das, H. Singh, S.K. Panda, N.M. Pugno, N.K. Katiyar, C.S. Tiwary, Unleashing enhanced yield strength: 3D printed octopus-inspired suction cups using topological engineering, *ACS Appl. Polym. Mater.* (2023), <https://doi.org/10.1021/acspolm.3c01721>.
- [8] R.L. Truby, J.A. Lewis, Printing soft matter in three dimensions, *Nature* 540 (2016) 371, <https://doi.org/10.1038/nature21003>.
- [9] M. Falahati, P. Ahmadvand, S. Safaei, Y.C. Chang, Z. Lyu, R. Chen, L. Li, Y. Lin, Smart polymers and nanocomposites for 3D and 4D printing, *Mater. Today* 40 (2020) 215, <https://doi.org/10.1016/j.mattod.2020.06.001>.
- [10] N.K. Bankapalli, V. Gupta, P. Saxena, A. Bajpai, C. Lahoda, J. Polte, Filament fabrication and subsequent additive manufacturing, debinding, and sintering for extrusion-based metal additive manufacturing and their applications: a review, *Compos. Part B Eng.* 264 (2023), 110915, <https://doi.org/10.1016/j.compositesb.2023.110915>.
- [11] R. Akman, H. Ramaraju, A. Verga, S.J. Hollister, Multimodal 3D printing of biodegradable shape memory elastomer resins for patient specific soft tissue repair, *Appl. Mater. Today* 29 (2022), 101666, <https://doi.org/10.1016/j.apmt.2022.101666>.
- [12] Z.N. Khan, H.I. Albalawi, A.U. Valle-Pérez, A. Aldoukhli, N. Hammad, E.H.P. d. León, S. Abdelrahman, C.A.E. Hauser, From 3D printed molds to bioprinted scaffolds: a hybrid material extrusion and vat polymerization bioprinting approach for soft matter constructs, *MSAM* 1 (2022), <https://doi.org/10.18063/msam.v1i1.7>.
- [13] P.S. Owuor, V. Chaudhary, C.F. Woellner, V. Sharma, R.V. Ramanujan, A. S. Stender, M. Soto, S. Ozden, E.V. Barrera, R. Vajtai, D.S. Galvão, J. Lou, C. S. Tiwary, P.M. Ajayan, High stiffness polymer composite with tunable transparency, *Mater. Today* 21 (2018) 475, <https://doi.org/10.1016/j.mattod.2017.12.004>.
- [14] L.R. Lopes, A.F. Silva, O.S. Carneiro, Multi-material 3D printing: The relevance of materials affinity on the boundary interface performance, *Addit. Manuf.* 23 (2018) 45, <https://doi.org/10.1016/j.addma.2018.06.027>.
- [15] A. Nazir, O. Gokcekaya, K. Md Masum Billah, O. Ertugrul, J. Jiang, J. Sun, S. Hussain, Multi-material additive manufacturing: a systematic review of design, properties, applications, challenges, and 3D printing of materials and cellular metamatials, *Mater. Des.* 226 (2023), 111661, <https://doi.org/10.1016/j.matedes.2023.111661>.
- [16] H. Jiang, P. Aihemaiti, W. Aiyiti, A. Kasimu, Study Of the compression behaviours of 3D-printed PEEK/CFR-PEEK sandwich composite structures, *Virtual Phys. Prototyp.* 17 (2022) 138, <https://doi.org/10.1080/17452759.2021.2014636>.
- [17] M.R. Khosrovani, P. Soltani, K. Weinberg, T. Reinicke, Structural integrity of adhesively bonded 3D-printed joints, *Polym. Test.* 100 (2021), 107262, <https://doi.org/10.1016/j.polymertesting.2021.107262>.
- [18] Z. Li, Z. Wang, W. Lu, X. Zhou, T. Suo, Loading rate dependence of mode II fracture toughness in laminated composites reinforced by carbon nanotube films, *Compos. Sci. Technol.* 215 (2021), 109005, <https://doi.org/10.1016/j.compscitech.2021.109005>.
- [19] R.S. Ambekar, I. Mohanty, S. Kishore, R. Das, V. Pal, B. Kushwaha, A.K. Roy, S. Kumar Kar, C.S. Tiwary, Atomic scale structure inspired 3D-printed porous structures with tunable mechanical response, *Adv. Engg. Mater.* 23 (2021), 2001428, <https://doi.org/10.1002/adem.202001428>.

- [20] E.F. Oliveira, R.S. Ambekar, D.S. Galvao, C.S. Tiwary, Schwarzites and schwarzynes based load-bear resistant 3D printed hierarchical structures, *Addit. Manuf.* 60 (2022), 103180, <https://doi.org/10.1016/j.addma.2022.103180>.
- [21] L.C. Felix, R.S. Ambekar, C.F. Woellner, B. Kushwaha, V. Pal, C.S. Tiwary, D. S. Galvao, Mechanical properties of 3D-printed pentadiamond, *J. Phys. D Appl. Phys.* 55 (2022), 465301, <https://doi.org/10.1088/1361-6463/ac91dc>.
- [22] R.S. Ambekar, B. Kushwaha, P. Sharma, F. Bosia, M. Fraldi, N.M. Pugno, C. S. Tiwary, Topologically engineered 3D printed architectures with superior mechanical strength, *Mater. Today* 48 (2021) 72, <https://doi.org/10.1016/j.mattod.2021.03.014>.
- [23] S.M. Sajadi, P.S. Owuor, S. Schara, C.F. Woellner, V. Rodrigues, R. Vajtai, J. Lou, D. S. Galvão, C.S. Tiwary, P.M. Ajayan, Multiscale geometric design principles applied to 3D printed schwartzites, *Adv. Mater.* 30 (2018), 1704820, <https://doi.org/10.1002/adma.201704820>.
- [24] C.S. Tiwary, S. Kishore, S. Sarkar, D.R. Mahapatra, P.M. Ajayan, K. Chattopadhyay, Morphogenesis and mechanostabilization of complex natural and 3D printed shapes, *Sci. Adv.* 1 (2023), e1400052, <https://doi.org/10.1126/sciadv.1400052>.
- [25] B. Kushwaha, K. Dwivedi, R.S. Ambekar, V. Pal, D.P. Jena, D.R. Mahapatra, C. S. Tiwary, Mechanical and acoustic behavior of 3D-printed hierarchical mathematical fractal merger sponge, *Adv. Eng. Mater.* 23 (2021), 2001471, <https://doi.org/10.1002/adem.202001471>.
- [26] S.M. Sajadi, P.S. Owuor, R. Vajtai, J. Lou, R.S. Ayyagari, C.S. Tiwary, P.M. Ajayan, Boxception: impact resistance structure using 3D printing, *Adv. Eng. Mater* 21 (2019), 1900167, <https://doi.org/10.1002/adem.201900167>.
- [27] L.C. Felix, C.F. Woellner, D.S. Galvao, Mechanical and energy-absorption properties of schwartzites, *Carbon* 157 (2020) 670, <https://doi.org/10.1016/j.carbon.2019.10.066>.
- [28] S.M. Sajadi, C.S. Tiwary, A.H. Rahmati, S.L. Eichmann, C.J. Thaemlitz, D. Salpekar, A.B. Puthirath, P.J. Boul, M.M. Rahman, A. Meiyazhagan, P.M. Ajayan, Deformation resilient cement structures using 3D-printed molds, *iScience* 24 (2021), 102174, <https://doi.org/10.1016/j.isci.2021.102174>.
- [29] S.M. Sajadi, C.F. Woellner, P. Ramesh, S.L. Eichmann, Q. Sun, P.J. Boul, C. J. Thaemlitz, M.M. Rahman, R.H. Baughman, D.S. Galvão, C.S. Tiwary, P. M. Ajayan, 3D printed tubulanes as lightweight hypervelocity impact resistant structures, *Small* 15 (2019), 1904747, <https://doi.org/10.1002/smll.201904747>.
- [30] B. Gupta, R.S. Ambekar, R.M. Tromer, P.S. Ghosal, R. Sinha, A. Majumder, P. Kumbhakar, P.M. Ajayan, D.S. Galvao, A.K. Gupta, C.S. Tiwary, Development of a schwartzite-based moving bed 3D printed water treatment system for nanoplastic remediation, *RSC Adv.* 11 (2021) 19788, <https://doi.org/10.1039/DRA03097C>.
- [31] P. Kumbhakar, R.S. Ambekar, P.L. Mahapatra, C. Sekhar Tiwary, Quantifying instant water cleaning efficiency using zinc oxide decorated complex 3D printed porous architectures, *J. Hazard. Mater.* 418 (2021), 126383, <https://doi.org/10.1016/j.jhazmat.2021.126383>.
- [32] S. AlZaid, N. Hammad, H.I. Albalawi, Z.N. Khan, E. Othman, C.A.E. Hauser, Advanced software development of 2D and 3D model visualization for TwinPrint, a dual-arm 3D bioprinting system for multi-material printing, *MSAM* 1 (2022), <https://doi.org/10.18063/msam.v1i3.19>.
- [33] Y. Xu, C. Wang, Y. Yang, H. Liu, Z. Xiong, T. Zhang, A multifunctional 3D bioprinting system for construction of complex tissue structure scaffolds: design and application, *MSAM* 8 (2022), <https://doi.org/10.18063/ijb.v8i4.617>.
- [34] G.D. Goh, S.L. Sing, Y.F. Lim, J.L.J. Thong, Z.K. Peh, S.R. Mogali, W.Y. Yeong, Machine learning for 3D printed multi-materials tissue-mimicking anatomical models, *Mater. Des.* 211 (2021), 110125, <https://doi.org/10.1016/j.matdes.2021.110125>.
- [35] W.L. Ng, T.C. Ayi, Y.C. Liu, S.L. Sing, W.Y. Yeong, B.H. Tan, Fabrication and characterization of 3D bioprinted triple-layered human alveolar lung models, *Int. J. Bioprint.* 7 (2021), <https://doi.org/10.18063/ijb.v7i2.332>.
- [36] ISO/TC 261 and ASTM Committee F42, ISO/ASTM 52900:2021 , Additive Manufacturing - General Principles - Fundamentals and Vocabulary, ISO, United Kingdom, 2021.
- [37] Y. Liu, S.L. Sing, A review of advances in additive manufacturing and the integration of high-performance polymers, alloys, and their composites, *MSAM* 2 (2023), <https://doi.org/10.36922/msam.1587>.
- [38] H. Terrones, M. Terrones, Curved nanostructured materials, *New J. Phys.* 5 (2003) 126, <https://doi.org/10.1088/1367-2630/5/1/126>.
- [39] K. Momma, F. Izumi, VESTA 3 for three-dimensional visualization of crystal, volumetric and morphology data, *J. Appl. Crystallogr.* 44 (2011) 1272, <https://doi.org/10.1107/S0021889811038970>.
- [40] P.G. Boyd, S.M. Moosavi, M. Witman, B. Smit, Force-field prediction of materials properties in metal-organic frameworks, *J. Phys. Chem. Lett.* 8 (2017) 357, <https://doi.org/10.1021/acs.jpclett.6b02532>.
- [41] A.K. Rappe, C.J. Casewit, K.S. Colwell, W.A. Goddard, W.M. Skiff, UFF, a full periodic table force field for molecular mechanics and molecular dynamics simulations, *J. Am. Chem. Soc.* 114 (1992) 10024, <https://doi.org/10.1021/ja00051a040>.
- [42] N. Ichihara, M. Ueda, 3D-printed high-toughness composite structures by anisotropic topology optimization, *Compos. Part B Eng.* 253 (2023), 110572, <https://doi.org/10.1016/j.compositesb.2023.110572>.
- [43] S. Gong, H. Ni, L. Jiang, Q. Cheng, Learning from nature: constructing high performance graphene-based nanocomposites, *Mater. Today* 20 (2017) 210, <https://doi.org/10.1016/j.mattod.2016.11.002>.